

Magneto-Actuated Reconfigurable Antennas on Hard-Magnetic Soft Substrates and E-Threads

Saad Alharbi, *Student Member, IEEE*, Qiji Ze, Ruike Zhao and Asimina Kiourti, *Senior Member, IEEE*

Abstract— We report new classes of reconfigurable antennas realized by embedding conductive e-threads inside programmable hard-magnetic soft substrates. Antenna deformations that rely on magnetic actuation are a promising alternative to conventional complicated and labor-intensive reconfiguration approaches due to their design, fabrication, and operation simplicity. However, state-of-the-art magneto-actuated approaches rely on soft-magnetic materials that suffer from stress failure, exhibit limited degrees of freedom, and do not allow programmable polarity deformations. Our work overcomes these challenges. By embedding NdFeB particles in soft silicone and by further coating e-thread antennas with the resulting flexible material, novel prototypes are brought forward that allow: programmable polarity, stable magnetic properties, untethered actuation, response speed could not be captured with high speed camera (60 frame per second), reversible deformation, light weight, and extreme mechanical/thermal tolerance. In this paper, we introduce the operating principle of this new class of antennas, optimize their fabrication, and validate them numerically and experimentally. As a proof-of-concept, validation is carried out for an accordion-based monopole, tunable from 680 to 835 MHz when actuated by a remote magnet. In future, this approach can be leveraged towards diverse reconfigurable antennas in consumer and defense applications.

Index Terms—Conductive threads, flexible antennas, reconfigurable antennas, magnetic substrate, textile antennas.

I. INTRODUCTION

ANTENNA reconfiguration in terms of operating frequency, polarization, radiation pattern and/or gain is becoming increasingly popular for diverse consumer and defense applications [1]-[5]. An indicative example comes from the area of wireless communications where a single reconfigurable antenna can be leveraged for multi-frequency connectivity, in turn reducing size and/or weight requirements. Antenna reconfiguration is typically accomplished by altering the current flow and electric field on the radiator element. As is well known, these can be controlled by modifying the

radiator's shape, material, size, placement, and so on [1]-[5].

Since 1931, when the idea of antenna reconfiguration was first introduced [6], [7], multiple reconfiguration techniques have been reported (electrical, mechanical, optical, material change, etc.). Referring to Table I, Micro-Electro-Mechanical System (MEMS) switches achieve low insertion loss and high linearity, but require high control voltages and raise reliability concerns inherent to the mechanical movement of the switches [1], [8], [9]. In other cases, ferrite materials are biased with relatively large DC voltages, magnetic or electric fields to dramatically increase their permittivity and enable high tunability. However, they suffer from severe bandwidth degradation and loss [10]-[12]. Plasma channel activation on high-resolution silicon using DC current injection can achieve significant operational flexibility and beam steering, but requires complex p-i-n biasing circuits and suffers from nonlinearity and low efficiency [13]. Mechanical approaches overcome several of these limitations, but raise concerns with the kinetic methods used for actuation. For instance, in [14], two large linear motion actuators were employed to move the ground plane and, hence, alter the thickness and frequency of a patch antenna. However, control of these actuators was highly complicated. Shape memory polymers (SMPs) can convert into pre-programmed structures via external stimuli [15], but have limited means of adhering to conductors. Instead, motors are often used to reshape the antennas, but such methods are bulky and power hungry [9], [4].

To avoid complexity inherent to the aforementioned methods, magneto-actuated reconfigurable antennas have been reported as a promising alternative [16]-[19]. In [16], a Plastic Deformation Magnetic Assembly (PDMA) was reported to realize an out-of-plane patch antenna. Fabrication relied on a thin layer of permalloy (magnetic material) coated on top of a patch antenna to plastically deform at an angle when subjected to an external static magnetic field. However, this approach was shown to suffer from stress failure at the joint and exhibited limited degrees of freedom. To overcome stress failure, a beam-steering antenna was reported in [17] that relied on a polymer-based hinge structure and Nickel as the magnetic actuator. However, this work achieved only a limited range of bending angles. Nickel was again used in [18] to move patch elements upon a pixelated antenna, but several shape restrictions were reported. At this point, it is worth noting that all these works [16]-[18] used soft-magnetic materials as actuators. These are known to exhibit high

Manuscript received June 28, 2019, revised February 1, 2020, revised March 18, 2020. Saad Alharbi is sponsored by King Abdulaziz City for Science and Technology.

S. Alharbi and A. Kiourti are with the ElectroScience Laboratory, Department of Electrical and Computer Engineering, The Ohio State University, Columbus, OH 43212 USA (e-mail: alharbi.75@osu.edu; kiourti.1@osu.edu).

Q. Ze and R. Zhao are with the Department of Mechanical and Aerospace Engineering, The Ohio State University, Columbus, OH 43210 USA (e-mail: ze.3@osu.edu; zhao.2885@osu.edu).

TABLE I
SUMMARY OF SOME OF RECONFIGURABLE ANTENNAS REPORTED IN THE LITERATURE VS. THE PROPOSED APPROACH

Ref.	Antenna Type	Freq. Range [GHz]	Reconfiguration Technique	Substrate/Conductive Surface	Advantages	Disadvantages
[9]	Patch	0.718 & 4.86	MEMS switch based (Electrical)	RO 4003/Copper	Wide bandwidth, low power consumption, reduced insertion loss, and high isolation	High control voltage, low reliability, limited lifecycle, and intensive labor work
[20]	Dipole	0.832 – 0.912	Switch Based (Thermal)	RF4/Copper	Low cost, low power consumption, and passive sensing	Discrete frequency change, nonlinear, high loss, and poor gain
[14]	Patch	2 – 6	Non-switch based (Mechanical)	RO 5880/Copper	Wide tuning range, stable radiation, and fixed radiation element	Bandwidth variation, non-sequential tuning, large overall size, and intensive labor work
[21]	Patch array	8.9 – 9.38	Non-switch Based (Material change)	Liquid crystal and RO 3003/Copper	Low cost, low loss, and insignificant change in radiation	Limited bandwidth, High biasing-control voltage, and intensive labor work
[22]	Patch	0.215 – 0.250	Non-switch Based (Material change)	Magnetic metamaterial and RO 4003/ Copper	Good miniaturization factors, and moderate loss	Low efficiency and bandwidth, and intensive labor work
[16]	Patch	25.6 – 28	Non-switch based (Magneto-Actuated /Mechanical)	Glass/ Copper (electroplated by permalloy)	Wide bandwidth, plastic deformation, high bending angle, and wide tuning	Poor cross-polarization, and stress failure at the flexed joined (poor lifecycle)
[17]	Patch array	57 – 61	Non-switch based (Magneto-Actuated /Mechanical)	Silicon polymer/ Electroplated gold	Beam steering, cost efficient, constant gain, and low loss	Limited bend angle range and intensive labor work
[18]	Patch array	1 – 8	Switch based (Magneto-Actuated /Mechanical)	RT Duroid/ Copper and Nickel	Eliminates pixelated antennas losses, wide beam scanning with different polarization, and wide tuning	Shape limited, limitation on the patches and switches locations, discrete tuning and intensive labor work
[19]	Dipole array	85-87.7	Non-switch based (Magneto-Actuated /Mechanical)	Silicon/ Electroplated gold on Co-Ni magnet layer	Large deflection under small magnetic field, wide bandwidth, and low power consumption	Limited frequency tune range, low Q factor, polarization effects, and intensive labor work
Proposed	Monopole	0.69 – 0.84	Non-switch Based (Magneto-Actuated /Mechanical)	Magneto-Actuated PDMS/ E-textile	Programmable polarity, stable magnetic properties, reversible deformation, not labor intensive, and mechanically/thermally robust	DC Magnetic field strength is directly proportional to the size of the antenna

permeability and low remanence values, and can only achieve the same polarity as the external magnetic field. In turn, a) easy demagnetization can occur that leads to potential failures and limits the range of applications, and b) shape reconfiguration modes are limited. Instead, in [19], a hard-magnetic material (40Co-60Ni) was used. This has a relatively higher remnant magnetization after being magnetized, hence allowing for significant angular deflections under a small magnetic field (<3 mT). Nevertheless, only one degree of freedom was reported. This is because the coercivity of 40Co-60Ni is only 5 kA/m, which gets it easily demagnetized by a relatively larger external magnetic field.

To overcome limitations in the state-of-the-art, we present new classes of magneto-actuated reconfigurable antennas that rely on conductive e-threads coated by programmable hard-magnetic soft substrates. The magnetic material we use is neodymium-iron-boron (NdFeB), which has high remnant magnetization (~863mT) and high coercivity (~732kA/m). By further embedding the NdFeB particles in soft silicone, and by utilizing the resulting flexible material to coat antennas realized on conductive e-threads, we enable novel magneto-actuated antenna prototypes that allow:

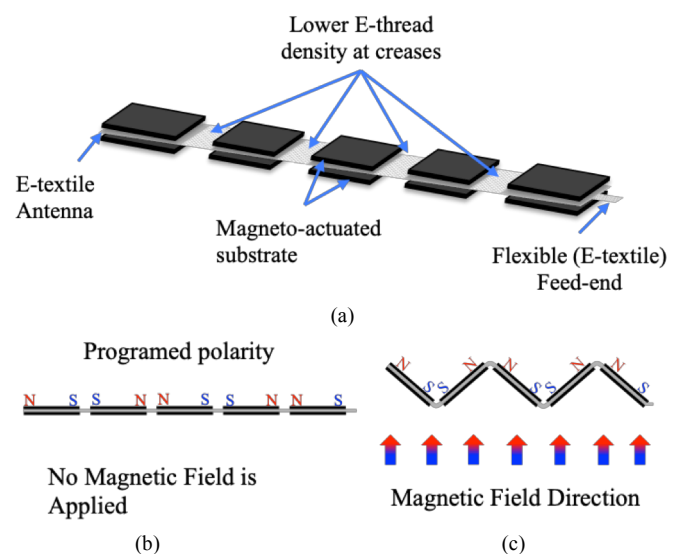


Fig. 1. Operating principle of the magneto-actuated e-textile antennas: (a) 3D block diagram of the integrated antenna, (b) side view of a programmed polarity magnetic material, and (c) programmed deformation by application of an exterior magnetic field.

programmable polarity, stable magnetic properties, untethered actuation, response speed could not be captured with our high speed camera with time resolution of 60 frame per second, reversible deformation, light weight, and extreme mechanical/thermal robustness. Notably, by controlling the NdFeB volume concentration, one may tune not just the magnetic properties, but also the dielectric properties and flexibility of the material. Here, our goal is to optimize the constituent materials of the newly reported antennas and their overall integration. As a proof-of-concept, an accordion-based magneto-actuated e-textile monopole is explored, tunable across ~680 to ~835 MHz when actuated by a remote magnet.

The rest of the paper is organized as follows. Section II introduces the operating principle of our magneto-actuated antennas. Section III describes formulation of the hard-magnetic soft material used to actuate the antenna and its magnetic and dielectric properties as a function of the NdFeB particle concentration. Section IV reports integration of the conductive material (e-textile) with the magneto-actuated substrate to form the end antenna. Validation for a proof-of-concept monopole is discussed in Section V. Mechanical and thermal testing is presented in Section VI, followed by discussion on multi-phase deformation capabilities in Section VII. The paper concludes in Section VIII.

II. OPERATING PRINCIPLE

The operating principle of the proposed magneto-actuated antennas is summarized in Fig. 1. As seen, a hard-magnetic soft material that can be readily actuated by a remote static magnetic field is adhered to an e-textile antenna to gain full control of its physical movement. For example, Fig. 1(a) shows a set-up where the e-textile antenna is sandwiched between two layers of magneto-actuated material. As will be discussed in Section IV, this integration technique has been identified as optimal in terms of the end prototype's versatility. When an external magnetic field is applied, the magnetic material and, hence, the integrated antenna deform based on: a) the programmed magnetic dipole moment inside the material (see Fig. 1(b)), and b) the field direction incident upon the material (see Fig. 1(c)). Consequently, changing the field direction further enables alternate shape control for the antenna, as will be discussed further in Section VII. It is noted that the magnetic field needs to be in place to keep the antenna in position; once the magnetic field is released, the antenna returns to its original state.

III. MAGNETO-ACTUATED MATERIAL

Programmed ferromagnetic domains embedded into an elastomer are employed to formulate the magneto-actuated material, in turn enabling high mechanical flexibility and fast 3D-shape transitions. Integration follows the method reported in [23], [24]. Specifically, the material is fabricated by embedding NdFeB microparticles into uncured silicone rubber (polydimethylsiloxane, PDMS). The mixture is cured at 70°C for 1 hr. After curing, the composite is magnetized under an impulse magnetic field (~1.5 T).

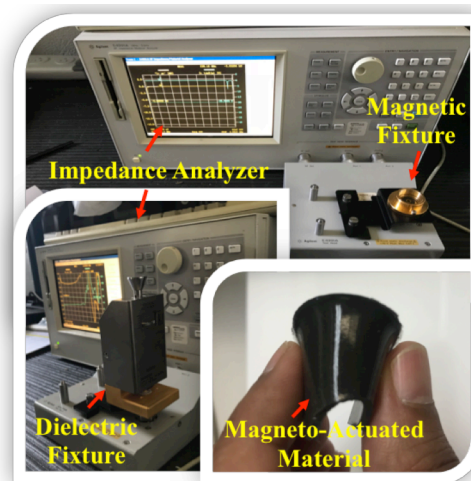


Fig. 2. Measurement set-up used to extract the dielectric and magnetic properties of the magneto-actuated substrate via fixtures connected to an impedance analyzer.

TABLE II
AVERAGE DIELECTRIC AND MAGNETIC PROPERTIES OF PURE MATERIALS FROM 1 MHz TO 1 GHz

Material	ϵ'_r	$\tan\delta_\epsilon$	μ'_r	$\tan\delta_\mu$
NdFeB	55.11	0.075	1.18	0.007
PDMS	3.11	0.005	1.00	0

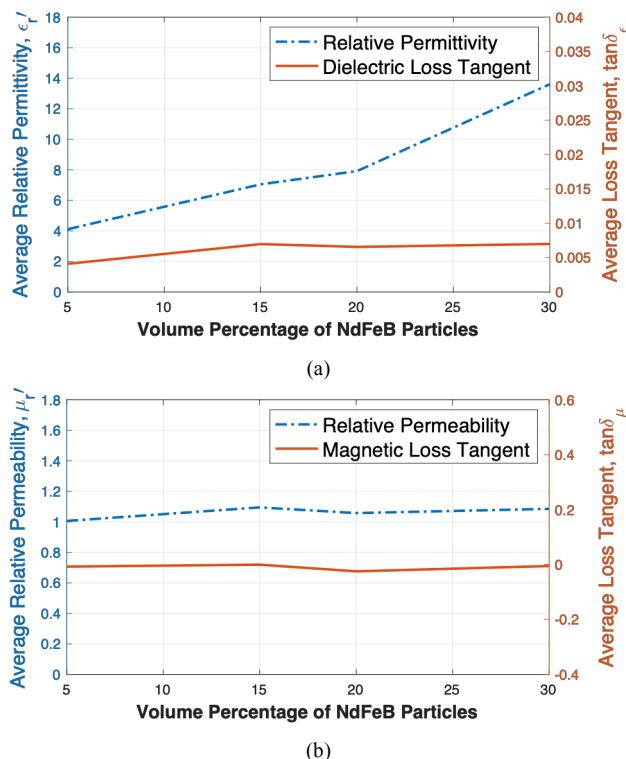


Fig. 3. Average properties as a function of volume percentage of NdFeB particles: (a) dielectric properties, and (b) magnetic properties.

The magnetic (relative permeability, μ'_r , magnetic loss tangent, $\tan\delta_\mu$) and dielectric (relative permittivity, ϵ'_r , dielectric loss tangent, $\tan\delta_\epsilon$) properties of the constituent materials and resulting magnetic composite elastomer are measured using a Keysight Impedance Analyzer (E4990A)

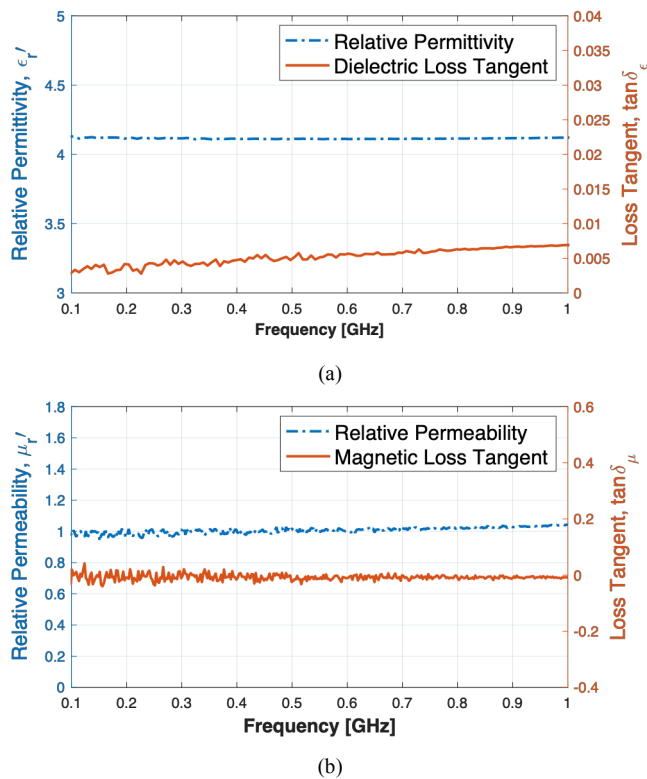


Fig. 4. Properties of 5 vol% sample as a function of frequency: (a) dielectric properties, and (b) magnetic properties.

equipped with a magnetic fixture (16454A) and a dielectric fixture (16453A), respectively (see Fig. 2). Measurements are reliable within the 1 MHz to 1 GHz frequency range, as attributed to the corresponding fixtures [25]. First, the pure materials (PDMS and NdFeB powder) are measured and averaged over the specified frequency range, Table II. Their values remain relatively constant within this frequency range, hence averaging provides for a good approximation. Then, four magnetic substrates, each with a different volume percentage of NdFeB particles (5, 15, 20, and 30 vol%) are formulated and measured. Their average properties over the aforementioned frequency range are plotted in Fig. 3, while properties as a function of frequency are indicatively plotted in Fig. 4 for the 5 vol% sample. Measurements are conducted several times for sample thicknesses varying from 1 mm to 3.5 mm to confirm repeatability of the results.

As seen, the 5 vol% sample demonstrates almost a fixed ϵ_r' of 4.11 and a varied $\tan\delta_\epsilon$ from 0.003 to 0.007 with an average of 0.004 across the specified frequency range. Because of this low value of $\tan\delta_\epsilon$, the material could readily be used as an antenna substrate without introducing significant loss. By homogeneously increasing the NdFeB particle concentration, ϵ_r' increases up to 13.60 for the 30 vol% sample, while there is no significant increase in $\tan\delta_\epsilon$. These properties can be leveraged to miniaturize the antenna size without apparent degradation in RF performance. It is worth noting, however, that a slight reduction in flexibility is noticed as the volume of magnetic particles increases. It is also noted that the value of μ_r' for the 5 vol% is very close to 1 across the measured frequency range and reaches its

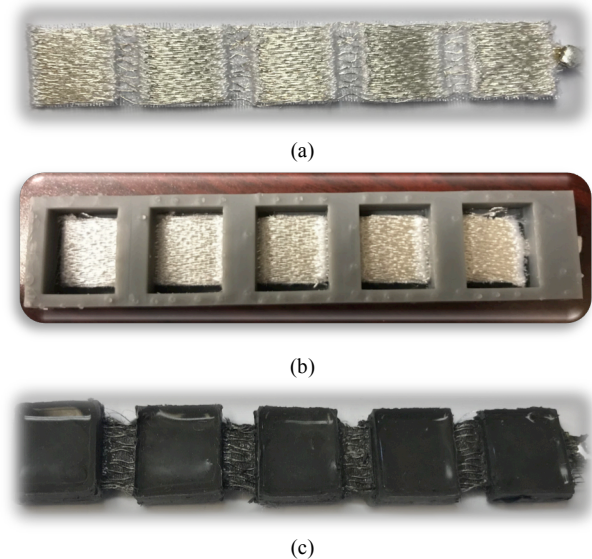


Fig. 5. Visualization of the antenna before and after the integration process: (a) graded e-textile antenna, (b) e-textile placed inside the 3D-printed mold before pouring the magnetic material, and (c) magneto-actuated e-textile after the integration process.

maximum (1.05) at the higher frequency end, Fig. 4(b). During calibration and without inserting any material inside the fixture, the value of $\tan\delta_\mu$ is fluctuating very close around zero and the behavior is similar after the material is placed inside the fixture per Fig. 4(b). These results are expected given that the employed magnetic particles (NdFeB) have μ_r' close to 1 and $\tan\delta_\mu$ close to zero, Table II.

IV. E-TEXTILE AND MAGNETIC MATERIAL INTEGRATION

Fabrication of the reported magneto-actuated antennas involves printing of the e-textile surface, followed by integration with the magnetic material. Here, automated embroidery of conductive e-threads is selected to realize the e-textile surface as attributed to its durability and robustness [26]. To further ease folding along the creases, a graded embroidery process is employed, as discussed in [27] and further illustrated for an example monopole antenna in Fig. 5(a). The 7-filament Elektrisola e-threads [28] that exhibit low DC resistance and very fine diameter of 0.12 mm are used in this work [29]. These e-threads have been shown to: a) achieve embroidery precision as high as ~ 0.1 mm, b) perform as good as copper up to a frequency of ~ 4 GHz [30], and c) exhibit high tolerance to mechanical stress and thermal deformation [26]. Several fabrics could be used during embroidery (e.g., Kevlar, cotton, or felt) and, accordingly, other conductive threads, besides Elektrisola, could be employed [31], [32]. Here, organza is selected as the underlying fabric given its light weight and its dielectric properties that are close to air (hence, not affecting the antenna performance in any way).

As a next step, integration of the e-textile surface with the magnetic material is pursued. For firm integration, the e-textile surface should be consolidated with the magnetic substrate during the material's curing process. After the material is cured, it would be difficult to maintain a solid

attachment to the e-textile because of the smoothness of the magnetic material surface. We also found that “sandwiching” the e-textile in between two layers of magnetic material provides much finer and much more accurate control over the bending process (see Fig. 1(a)). To achieve equivalent performance with just a single substrate layer, the corresponding layer thickness should be significantly increased. In turn, this would increase the overall antenna size and weight. Added to the above, the reported “sandwiching” approach serves to protect the e-textile surface from wear and corrosion. Finally, we found that applying the magnetic material at the non-crease areas only provides the best mechanical movement for the end prototype and, most importantly, a complete reverse transition to the initial state when the magnetic field is released (i.e., back to flat).

For fabrication, the 3D-printed mold of Fig. 5(b) is employed where the antenna is placed in the middle and the magnetic material is poured through the designed upper holes. To facilitate extraction of the prototype after curing, the surface of the mold is coated with silicone release agent. Fig. 5(c) shows the magneto-actuated e-textile after completion of the integration process.

V. VALIDATION FOR A PROOF-OF-CONCEPT MONOPOLE

A. Antenna Design

As a proof-of-concept, a quarter-wavelength monopole is considered, designed to resonate at 790 MHz when operating in free-space (i.e., when not coated with magnetic material). This selection is considered because of: a) the simplicity in fabrication and integration associated with monopole designs, and b) the feasibility of operation in the lower band of the ultra high frequency (UHF) range where material properties have accurately been measured. The prototype is shown in Fig. 5(a) and exhibits a length of 82 mm, a width of 10 mm, and four creases placed equally across its length. The crease length is set to 5 mm and the graded embroidery alternates between 7 e-threads/mm and 1 e-thread/mm. Such choices rely on mechanical performance criteria that will be discussed in detail in Section VI. Following embroidery, the integration process of Section IV is pursued with the 20 vol% magnetic material being selected as a compromise between the exhibited flexibility and dielectric/magnetic properties. The final integrated prototype is shown in Fig. 5(c) and exhibits an overall thickness of 2 mm.

To complete the monopole, the magneto-actuated e-textile radiator element is further integrated with a large square copper ground plane (~305 mm in length). At the gap between the antenna and ground plane, a 50 Ω SMA connector is attached. Because of the flexibility of the e-textile, a cardboard is placed as a surface perpendicular to the ground plane to support the radiator element, see Fig. 6 (a).

B. Antenna Performance when Flat

The magneto-actuated e-textile monopole is first evaluated when flat and without any magnetic field involved. For comparison, the equivalent e-textile antenna without the magnetic substrate is also fabricated and measured. Finite

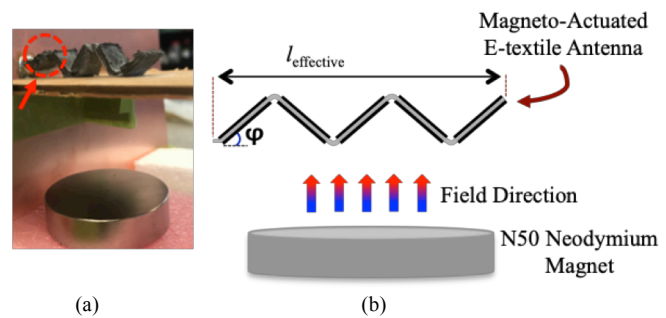


Fig. 6. Magneto-actuated e-textile subject to the magnetic field of a grade N50 Neodymium magnet: (a) actual view, and (b) illustration diagram including the definition of the bend angle (ϕ).

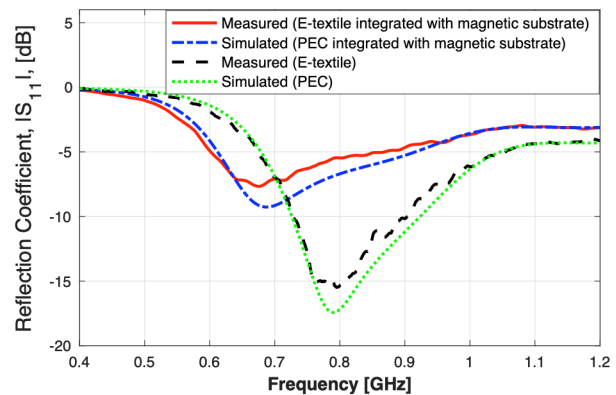


Fig. 7. Comparison of the measured and simulated reflection coefficient, $|S_{11}|$, for the monopole antenna when lying flat. Two scenarios are shown, with the e-textile covered with the magnetic material and not.

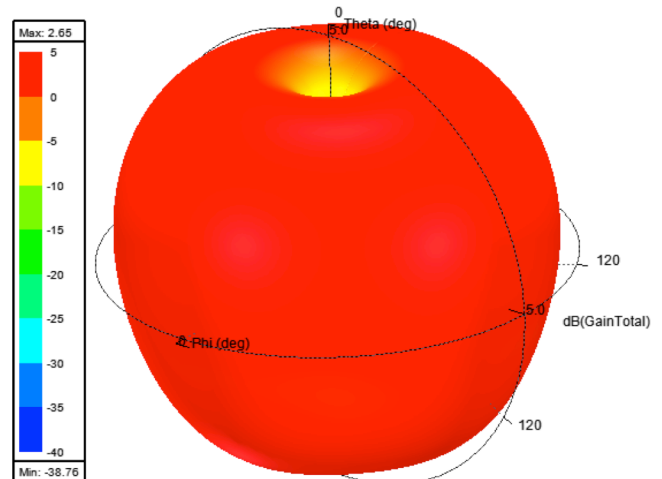


Fig. 8. Simulated radiation pattern of the e-textile monopole covered with 20 vol% magnetic material (at the corresponding resonance frequency).

Element (FE) simulations are further carried out in ANSYS HFSS [33] considering the Perfect Electric Conductor (PEC) equivalents of these antennas.

As shown in Fig. 7, reflection coefficient ($|S_{11}|$) measurements are in good agreement with simulations. In the absence of any magnetic material, the antenna resonates at ~790 MHz. When the magnetic material is integrated, the resonance frequency reduces to ~680 MHz, the 6-dB bandwidth increased by ~20%, and $|S_{11}|$ at resonance reduces by ~6 dB. Such performance is expected given the high

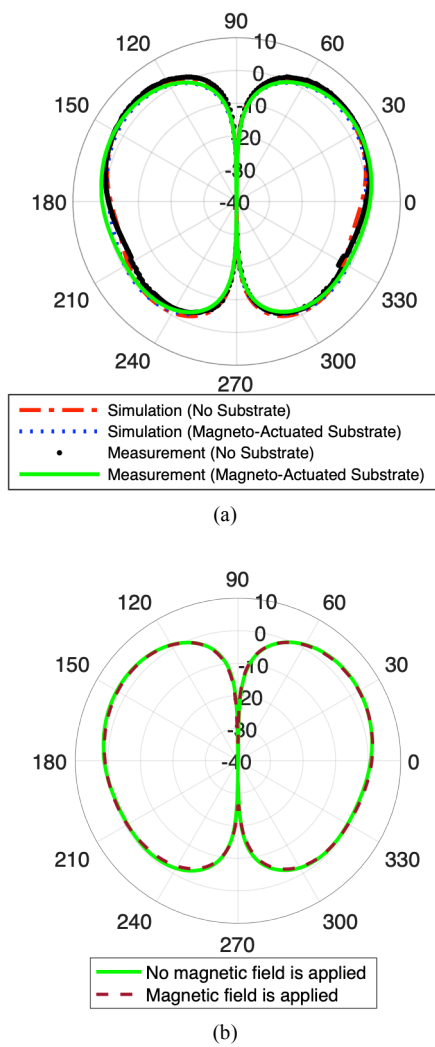


Fig. 9. E-plane radiation patterns of e-textile monopoles covered with magnetic material and not (at the corresponding resonance frequencies): (a) simulated and measured without the magnetic field effects, and (b) measured with and without the magnetic field effects.

permittivity associated with the magnetic material. Since this is a proof-of-concept demonstration, better matching of the integrated antenna is outside the scope of this work.

The far-field radiation pattern and gain performance are further explored. Referring to Fig. 8, the simulated 3D radiation pattern for the prototype covered with 20 vol% magnetic material demonstrates an almost donut shape. To better understand the effect of the magnetic material, Fig. 9(a) compares the measured and simulated E-plane radiation patterns for prototypes: (a) covered with magnetic material and (b) uncovered. As seen, excellent agreement is observed. As a further study, Fig. 9(b) compares the measured antenna radiation pattern: (a) without the DC magnetic field, and (b) when the DC magnetic field is applied. Again, excellent agreement is achieved. In all cases, the patterns are plotted at the corresponding resonance frequencies.

Having verified consistency between measurements and simulations, the radiation efficiency is examined numerically. Only $\sim 1\%$ difference in radiation efficiency is observed with and without the magnetic material. This is expected given the

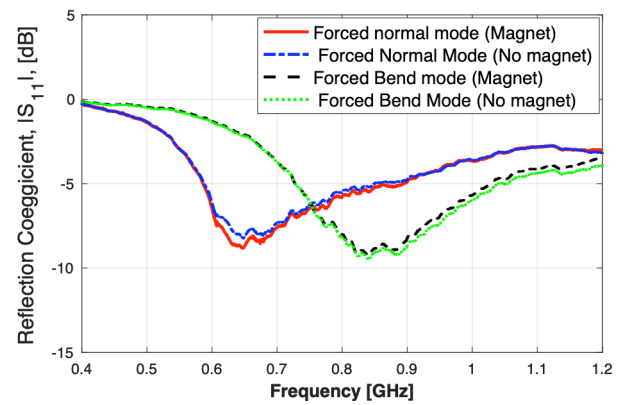


Fig. 10. Comparison of the measured reflection coefficient, $|S_{11}|$, for the magneto-actuated e-textile monopole when forced flat and bent, and while applying or releasing the magnetic field.

TABLE III
COMPARISON BETWEEN SIMULATION AND MEASUREMENT RESULTS FOR DIVERSE SPACING BETWEEN THE ANTENNA AND MAGNET

Magnet Position	Spacing from Antenna (mm)	Bending Angle (Degrees)	Measured Shift in resonant frequency (%)	Simulated Shift in resonant frequency (%)
1	97.5	9.07	0.83	1.16
2	67.5	12.84	5.26	2.6
3	47.5	36.87	14.91	15.9
4	27.5	44.56	22.79	21.68

low loss of our magnetic material.

C. Reconfiguration Performance

To assess the antenna performance during diverse reconfiguration stages, a DC magnetic field needs to be employed. Here, the DC magnetic field is generated using a strong disk permanent magnet, viz. Neodymium magnet of grade N50 per Fig. 6. The magnet has an overall diameter of ~ 50 mm and a thickness of ~ 20 mm, and generates a surface magnetic flux density of ~ 300 mT [34]. Because of the high electrical conductivity of the Neodymium magnet ($\sigma = 10^6$ S/m) [34], the magnet may have great influence on the antenna performance when in touch with the ground plane. Numerical studies indicate that the ground-to-magnet distance needed to avoid any undesired loading is ~ 1 cm. Although the position of the magnet to the radiator element has effects on the antenna performance, experimental results in Fig. 10 confirm how a magnet placed at 6.75 cm away from the antenna does not load it any way. Here, the e-textile monopole is first measured in the presence of the magnet but forced securely flat via a lossless tape that has permittivity close to air. Then, the magnetic field is released and the reflection coefficient is measured again. Similar measurements are conducted while the antenna is forced at ~ 55 degrees bending angle (per definition in Fig. 6(b)), with results confirming identical performance in the presence or absence of a magnet. These results not only indicate that the antenna is not loaded by the magnet, but further confirm that the external magnetic field does not alter the properties of the magnetic material. It is, hence, demonstrated that the hard-magnetic material (NdFeB) has a permeability that remains close to 1 upon application of

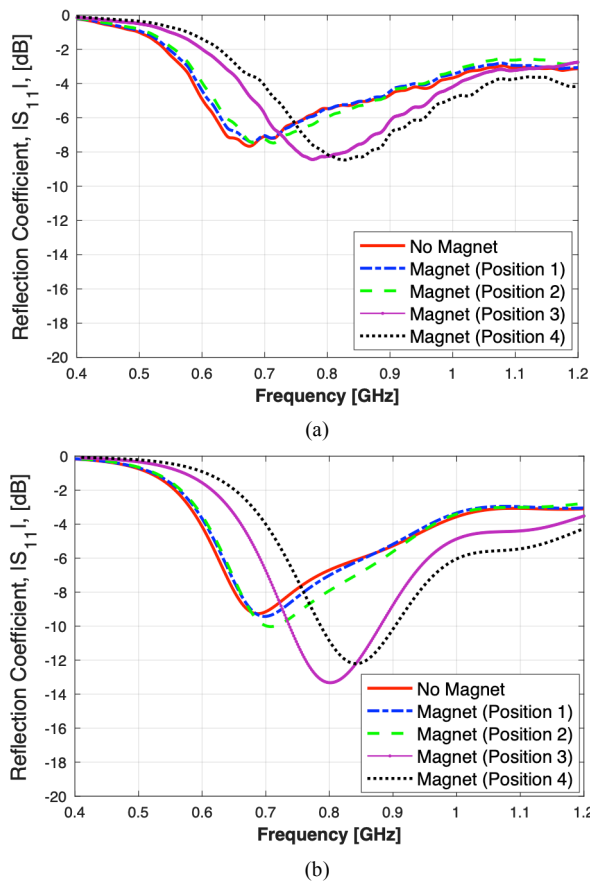


Fig. 11. Reflection coefficient, $|S_{11}|$, of the magneto-actuated e-textile monopole confirming reconfiguration under varying positions of the magnet, or, equivalently, magnitude of the magnetic field: (a) measurements, and (b) simulations.

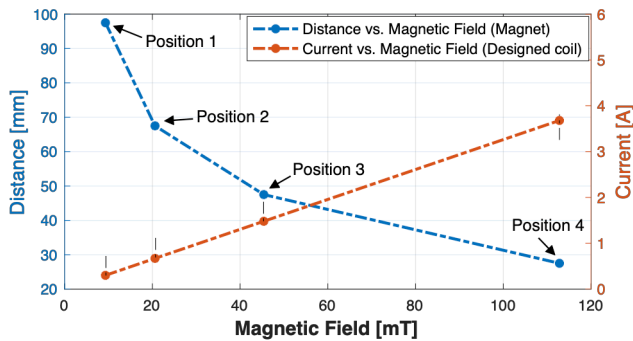


Fig. 12. The measured magnetic field of the N50 neodymium magnet at different distance from the antenna (positions 1-4 as indicated in Table III) and the required current for the designed coil to generate a similar magnetic field at a fixed distance of 20 mm.

the magnetic field (unlike soft-magnetic materials).

As expected, Fig. 10 further shows that the frequency is shifted based on the physical movement of the radiator element. Specifically, a 30% change in resonance frequency is observed by the employed 55 degree bending. This confirms the intended reconfiguration performance. To further explore the antenna performance as a function of different reconfiguration stages, we design a fixture with four fixed positions for the magnet to sit on, see Table III. The closer the magnet gets to the antenna, the stronger the magnetic field becomes, and the antenna folds in a more pronounced way.

The measured bending angle (φ), defined in Fig. 6, increases as $\varphi = 9.07^\circ$, 12.84° , 36.87° and 44.56° for positions 1, 2, 3 and 4, respectively. These values of φ are calculated assuming a completely uniform flexion, measuring the effective length of the antenna after deformation ($l_{effective}$), and further using Eq. (1):

$$\varphi = \cos^{-1} \left(\frac{l_{effective}}{l} \right) \quad (1)$$

where l is the overall length of the antenna when flat. Here, it is worth noting a slight limitation in the flexion capabilities of the employed prototype. Specifically, the monopole is connected to an SMA connector and the ground plane on one end so that when the magnetic field is applied, its two ends cannot pull equally to form a uniform shape. To overcome this limitation, a small amount of astringent powder is sprinkled on top of the cardboard surface. Also, a small separation is created between the feed and the supporting cardboard, as shown in Fig. 6(a), to reduce the stress on the antenna.

As the field strength increases and the antenna folds accordingly, the resonance frequency shifts to higher values. Measured and simulated reflection coefficients for each of the four magnet positions reported in Table III are shown in Fig. 11(a) and (b), respectively. Table III further compares the percentage shift in resonance frequency for the aforementioned cases. Theoretically, as the monopole folds in free space, its impedance becomes lower and an increase in mismatch loss is expected. This behavior is verified in [35]. However, here, the PDMS and magnet properties change the impedance behavior of the antenna. As such, better matching is achieved at higher folding angles as shown in Fig. 11(a) and (b).

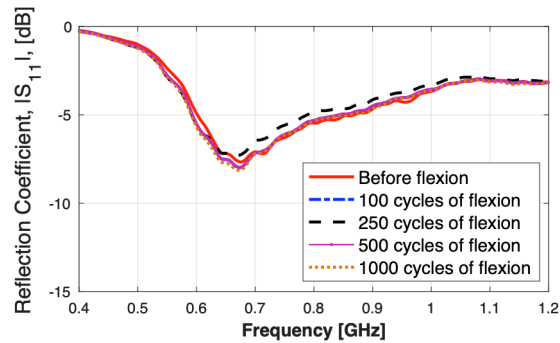
D. Speed of Configuration and Coil Analysis

The configuration speed of the antenna is analyzed upon application of the magnetic field. The exact time measured to deform the designed structure is 0.7 sec using video recording with a camera that captures 60 frames per second. However, this measured time relates to the speed of the hand required to place the magnet at the right location. Other than that, our camera could not capture the real deformation speed. Consequently, we estimated the time required for reconfiguration relates to the time needed to deliver the intended magnetic field. For example, if a coil is used (instead of a magnet), the reconfiguration time will equal the time needed for the current delivered to the coil to generate the magnetic field. For comparison, the speed for MEMS-based reconfiguration techniques depends on the switching time of MEMS, which ranges from 1-200 μsec [3].

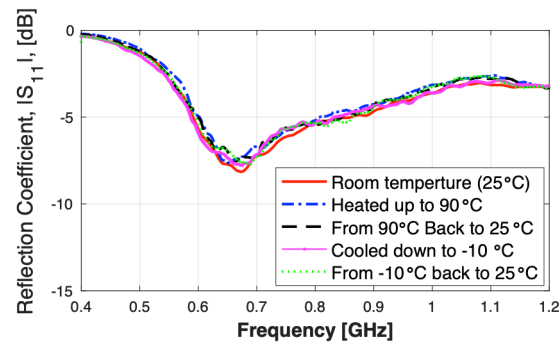
In a practical system, a magnet may not be feasible and a coil may need to be employed instead to generate the required magnetic field. For example, Fig. 12 shows the magnetic field generated by our magnet in our proof-of-concept set-up, as it moves towards the antenna across positions 1, 2, 3, and 4, reported in Table III. As expected, the closer the magnet is to the antenna, the stronger the magnetic field. For example, referring to position 4, the magnetic field is 112.8 mT. If this

TABLE IV
COMPARISON BETWEEN THE FOUR DIFFERENT PROTOTYPES IN TERMS OF
THE ACHIEVED DEFORMATION PERFORMANCE

Prototype	Bending Angle (degrees)			
	Position 1	Position 2	Position 3	Position 4
1	6.49	9.18	20.63	24.46
2	9.07	11.11	33.12	40.31
3	6.49	9.18	22.62	27.80
4	9.07	12.84	36.87	44.56



(a)



(b)

Fig. 13. Reflection coefficient, $|S_{11}|$, for the magneto-actuated e-textile monopole during: (a) mechanical testing, and (b) thermal testing.

same magnetic field but at fixed distance (20 mm) were to be generated by a coil, an example implementation could entail a coil of 0.5 mm in wire diameter, 20 mm in inner diameter, and 84 mm in outer diameter, fed by 3.68 A. Here, it is worth noting that the magnetic field required to achieve the deformation depends on the antenna design and its deformation behavior. In our proof of concept implementation, the antenna design is large in size and its deformation behavior is always pulled from one side; hence a relatively large magnetic field is required, as indicated above.

VI. MECHANICAL AND THERMAL TESTING

A. Mechanical Testing

Two tests are conducted to explore the mechanical performance of the integrated magneto-actuated e-textile antenna. The first test focuses on the deformation agility of the prototype while varying: a) the density of embroidered e-threads along the creases, and b) the length of the gap around the creases that exhibits reduced embroidery density. Here, deformation agility is defined as the prototype's ability to achieve a larger bending angle under the same magnetic field, while still maintaining uniform folding across its length

and the ability to return back to its initial state as soon as the field is released. To this end, four prototypes are fabricated. Referring to Table IV, prototypes 1 and 2 employ a density of a 7 e-threads/mm upon the antenna surface and a reduced density of 4 and 1 e-threads/mm along a 2.5mm-length upon the creases, respectively. Prototypes 3 and 4 employ a density of a 7 e-threads/mm upon the antenna surface and a reduced density of 4 and 1 e-threads/mm along a 5mm-length upon the creases, respectively. All four prototypes are coated with 20 vol% magnetic material per the process outlined in Fig. 5. Their bending angle is then measured (per Eq. (1)) when the magnet of Fig. 6(b) is positioned at each of the four locations indicated in Table III.

Results are summarized in Table IV. As seen, prototype 2 and 4 achieve larger bending angles. This is attributed to the higher flexibility obtained by lowering the e-thread density. It is also noted that the wider length of reduced embroidery density along the creases associated with prototype 4 enables the largest bending angles. By contrast, consecutive magnetic substrate sectors in prototype 2 end up touching each other at relatively smaller bending angles. Added to the above, prototypes 2 and 4 show much better recovery back to their original flat state after releasing the magnetic source. This is attributed to the ability of the organza substrate to recover back to the original flat state since, at lower e-thread density, movement is not dominated by the e-thread but rather the fabric itself. By contrast, at higher density, the antenna needs to be manually forced back to flat as attributed to the rigidity of the e-thread surface. Alternatively, full recovery back to flat mode can be achieved by applying negative (opposite direction) magnetic fields.

Building on the above, prototype 4 is hereafter selected as optimal and further used in the second round of mechanical tests. These latter tests aim to examine robustness of the prototype during lifelong deformations. More specifically, in this experiment, we focus on the consistency of the antenna's RF performance as a function of bending cycles. To this end, 1000 cycles of flexion are enforced for the prototype by placing the magnet at a distance of 2.75 cm, releasing it, and then repeating the process by 1000 times. The reflection coefficient, $|S_{11}|$, recorded during this flexion process is shown in Fig. 13(a). As seen, extreme tolerance to bending is identified with only a ± 0.3 dB difference recorded between readings. Furthermore, there are no signs of damage or wear on the creases even after 1000 deformation cycles.

B. Thermal Testing

To confirm unaltered performance at high/low temperatures, the antenna reflection coefficient is measured while subject to temperatures of -10°C to 90°C . To this end, the antenna prototype is measured at room temperature (25°C) and further placed on a hot plate until its internal temperature reaches 90°C . The antenna performance is measured at that instant and is then left to cool down to room temperature when it is measured again. The antenna is then placed in a freezer until it reaches -10°C and measured again. Similarly, it is left to return back to room temperature and re-measured. Referring

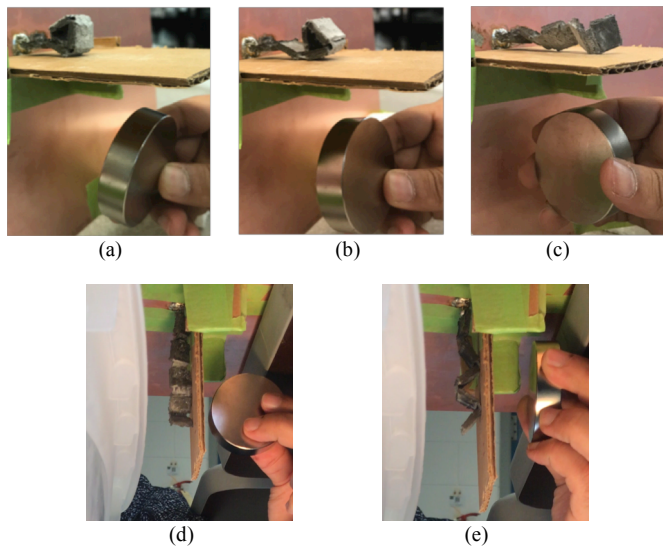


Fig. 14. Multi-phase deformation using varying orientation of the magnet to: (a) fold, (b) unfold, (c) twist the antenna prototype, (d) vertical twist, and (e) vertical bend.

to Fig. 13(b), the antenna demonstrates high thermal tolerance, confirming its suitability for diverse defense and consumer applications.

It is worth noting here that the experimental results of Fig. 13(b) are not hot/cold storage tests, but rather real-time monitoring of antenna prototypes subject to the corresponding temperatures. As such, temperatures below -10°C were not feasible with our existing set-up but can be explored in future.

VII. MULTI-PHASE DEFORMATION

Our work so far explored deformation of the magneto-actuated material and embedded antenna in an accordion configuration. However, it is worth noting that more complex shape deformations can be achieved based on the programmed polarity of the material and its interaction with the external magnetic field (i.e., field strength and direction). Accordingly, multiple deformations can be enabled for even the same prototype. For example, by re-orienting the magnet in a step-by-step manner, the monopole prototype of Fig. 5(c) can eventually be rolled (Fig. 14(a)) and unrolled (Fig. 14(b)). Another type of ‘twisting’ deformation may be achieved via an alternate orientation of the magnet, Fig. 14(c). A vertical twist and bending are shown in Fig. 14(d) and (e) to confirm that the deformation is fully controlled by the magnetic field. That is, materials, antennas, and external magnetic fields can carefully be engineered to achieve multi-phase deformations, suitable for diverse applications in future.

VIII. CONCLUSION

A novel class of mechanically reconfigurable antennas was presented that overcomes limitations in state-of-the-art magneto-actuated prototypes. Classical ways of non-antenna-based reconfiguration, such as PIN or varactor diodes or FETs, suffer from several disadvantages, such as the need for high control voltages or currents, poor quality factors, complex bias and control circuits, and so on. Our proposed approach envisions to overcome such limitations. It relies on integration of preprogrammed magneto-actuate materials with embroidered

e-textile antennas, and is carefully optimized for enhanced flexibility, reversible deformation, and high mechanical and thermal tolerance. Feasibility of the proposed approach was demonstrated via a proof-of-concept accordion-based monopole actuated by a magnet in close proximity. By remotely actuating the monopole to fold in an accordion-based manner, its resonant frequency shifted from ~ 680 to ~ 830 MHz and its 6-dB bandwidth increased by $\sim 20\%$. Even more importantly, results indicated that the reported approach: a) does not suffer from stress failure, b) may exhibit numerous degrees of freedom (achieved by altering the material composition and magnetic field direction and strength), c) is stable (because of the hard-magnetic soft material used), and d) allows programmed polarity to achieve multi-phase desired deformation. In future, the aforementioned characteristics may be leveraged to design more sophisticated antennas for diverse consumer and defense applications. Specifically, our future work aims to design a practical antenna with multi-deformation performance using a practical actuation system and will, in turn, involve much more in-depth comparison vs. prior techniques (including power consumption, speed of configuration, circuit and antenna size, etc.).

REFERENCES

- [1] N. Haider, D. Caratelli, and A. G. Yarovoy, “Recent developments in reconfigurable and multiband antenna technology,” *International Journal of Antennas and Propagation*, pp.1-14, 2013.
- [2] R. L. Haupt and M. Lanagan, “Reconfigurable antennas,” *IEEE Antennas and Propagation Magazine*, vol. 55, no. 1, pp. 49-61, Feb. 2013.
- [3] J. Costantine, Y. Tawk, S. E. Barbin, C. G. Christodoulou, “Reconfigurable antennas: Design and applications,” *Proceeding of the IEEE*, vol. 103, no. 3, pp. 424-437, Mar. 2015.
- [4] S.M. Saeed, C.A. Balanis, C.R. Birtcher, A.C. Durgun, and H.N. Shaman, “Wearable flexible reconfigurable antenna integrated with artificial magnetic conductor,” *IEEE Antennas Wireless Propag. Lett.*, vol. 16, pp. 2396-2399, Jun. 2017.
- [5] N. O. Parchin, H. J. Basherlou, Y. Al-Yasir, R. Abd-Alhameed, A. Abdulkhaleq, and J. Noras, “Recent Developments of Reconfigurable Antennas for Current and Future Wireless Communication Systems,” *Electronics*, vol. 8, no. 2, p. 128, 2019.
- [6] E. Bruce, “Developments in Short-Wave Directive Antennas*,” *Bell System Technical Journal*, vol. 10, no. 4, pp. 656-683, 1931.
- [7] E. Bruce and A. C. Beck, “Experiments with Directivity Steering for Fading Reduction,” *Bell System Technical Journal*, vol. 14, no. 2, pp. 195-210, April 1935.
- [8] G. H. Huff and J. T. Bernhard, “Integration of packaged RF MEMS switches with radiation pattern reconfigurable square spiral microstrip antennas,” *IEEE Trans. on Antennas and Propag.*, vol. 54, no. 2, pp. 464-469, Feb. 2006.
- [9] A. Zohur, H. Mopidevi, D. Rodrigo, M. Unlu, L. Jofre, and B. A. Cetiner, “RF MEMS Reconfigurable Two-Band Antenna,” *IEEE Antennas Wireless Propag. Lett.*, vol. 12, pp. 72-75, 2013.
- [10] D. M. Pozar and V. Sanchez, “Magnetic tuning of a microstrip antenna on a ferrite substrate,” *Electronics Letters*, vol. 24, no. 12, pp. 729-731, Jun. 1988.
- [11] G. Yang et al., “Tunable miniaturized patch antennas with self-biased multilayer magnetic films,” *IEEE Trans. on Antennas and Propag.*, vol. 57, no. 7, pp. 2190-2193, July 2009.
- [12] E. Andreou, T. Zervos, A. A. Alexandridis and G. Fikioris, “Magneto-dielectric materials in antenna design: Exploring the potentials for reconfigurability,” *IEEE Antennas and Propagation Magazine*, vol. 61, no. 1, pp. 29-40, Feb. 2019.
- [13] A. E. Fathy et al., “Silicon-based reconfigurable antennas-concepts, analysis, implementation, and feasibility,” *IEEE Trans. Microw. Theory and Techn.*, vol. 51, no. 6, pp. 1650-1661, June 2003.

- [14] J. Costantine, Y. Tawk, J. Woodland, N. Flaum and C. G. Christodoulou, "Reconfigurable antenna system with a movable ground plane for cognitive radio," *IET Microwaves, Antennas & Propagation*, vol. 8, no. 11, pp. 858-863, 19 August 2014.
- [15] G. J. Hayes, Y. Liu, J. Genzer, G. Lazzi and M. D. Dickey, "Self-Folding Origami Microstrip Antennas," *IEEE Trans. on Antennas and Propag.*, vol. 62, no. 10, pp. 5416-5419, Oct. 2014.
- [16] J. -C. Langer, J. Zou, C. Liu and J. T. Bernhard, "Micromachined reconfigurable out-of-plane microstrip patch antenna using plastic deformation magnetic actuation," *IEEE Microw. Wireless Compon. Lett.*, vol. 13, no. 3, pp. 120-122, March 2003.
- [17] C.-W. Baek, S. Song, J.-H. Park, S. Lee, J.-M. Kim, W. Choi, C. Cheon, Y.-K. Kim, and Y. Kwon, "A V-band micromachined 2-D beam-steering antenna driven by magnetic force with polymer-based hinges," *IEEE Trans. Microw. Theory and Techn.*, vol. 51, no. 1, pp. 325-331, 2003.
- [18] J. Pal, F. Donzelli, D. Piazza, J. A. Bain, and G. Piazza, "Magnetically reconfigurable pixelated antenna," *Microwave and Optical Technology Letters*, pp. 1-6, 2019.
- [19] J. M. Zendejas, J. P. Gianvittorio, Y. Rahmat-Samii and J. W. Judy, "Magnetic MEMS reconfigurable frequency-selective surfaces," *Journal of Microelectromechanical Systems*, vol. 15, no. 3, pp. 613-623, June 2006.
- [20] Z. Jiang and F. Yang, "Reconfigurable Sensing Antennas Integrated With Thermal Switches for Wireless Temperature Monitoring," *IEEE Antennas Wireless Propag. Lett.*, vol. 12, pp. 914-917, 2013.
- [21] F. N. Ayoub, C. D. Woehrle, Y. Tawk, D. Doyle, C. G. Christodoulou, and J. Costantine, "Frequency-tunable patch array using highly anisotropic liquid crystal," *Proc. APSURSI*, pp. 1664-1665, 2014.
- [22] K. Buell, H. Mosallaei and K. Sarabandi, "A substrate for small patch antennas providing tunable miniaturization factors," *IEEE Trans. Microw. Theory and Techn.*, vol. 54, no. 1, pp. 135-146, Jan. 2006.
- [23] R. Zhao, Y. Kim, S. A. Chester, P. Sharma, and X. Zhao, "Mechanics of hard-magnetic soft materials," *Journal of the Mechanics and Physics of Solids*, vol. 124, pp. 244-263, 2019.
- [24] Y. Kim, H. Yuk, R. Zhao, S. A. Chester, and X. Zhao, "Printing ferromagnetic domains for untethered fast-transforming soft materials," *Nature*, vol. 558, no. 7709, pp. 274-279, 2018.
- [25] Literature.cdn.keysight.com. (2019). [online] Available at: <http://literature.cdn.keysight.com/litweb/pdf/5991-3888EN.pdf>
- [26] J. Zhong, A. Kiourti, T. Sebastian, Y. Bayram, and J.L. Volakis, "Conformal load-bearing spiral antenna on conductive textile threads," *IEEE Antennas Wireless Propag. Lett.*, pp. 230-233, May 2016.
- [27] S. Alharbi, S. Chaudhari, A. Inshaar, H. Shah, C. Zou, R. L. Harne, and A. Kiourti, "E-Textile Origami Dipole Antennas With Graded Embroidery for Adaptive RF Performance," *IEEE Antennas Wireless Propag. Lett.*, vol. 17, no. 12, pp. 2218-2222, 2018.
- [28] Electrisola Feindraht AG Textile Wire. [online] Available at: <http://www.textile-wire.ch/>
- [29] A. Kiourti, C. Lee, and J.L. Volakis, "Fabrication of textile antennas and circuits with 0.1mm precision," *IEEE Antennas Wireless Propag. Lett.*, vol. 15, pp. 151-153, 2015.
- [30] A. Kiourti and J.L. Volakis, "High geometrical accuracy embroidery process for textile antennas with fine details," *IEEE Antennas Wireless Propag. Lett.*, vol. 14, pp. 1474-1477, 2015.
- [31] K. Karlsson, J. Carlsson, "Wideband characterization of fabrics for textile antennas", 2012 6th in *European Conference on Antennas and Propagation EuCAP*, Prague, Czech Republic, pp. 1358 - 1361, 2012.
- [32] B. Ivsic, D. Bonefacic, J. Bartolic, "Considerations of embroidered textile antennas for wearable applications", *IEEE Antennas and Wireless Propag. Lett.*, Vol.12, pp.1708 - 1711, 2013.
- [33] Ansys High Frequency Structure Simulator. [online] Available at: <https://www.ansys.com/products/electronics/ansys-hfss>
- [34] Eclipsemagnetics.com. (2019). [online] Available at: <https://www.eclipsemagnetics.com/media/wysiwyg/datasheets/magnet-materials-and-assemblies/ndfeb-neodymium-iron-boron-standard-ndfeb-range-datasheet-rev1.pdf>.
- [35] S. Alharbi, and A. Kiourti, "Folding-Dependent vs. Folding-Independent Flexible Antennas on E-Textiles," 2019 *IEEE International Symposium on Antennas and Propagation & USNC/URSI National Radio Science Meeting*, Atlanta, GA, pp. 755-756, 2019.



Saad Alharbi (S'16) received the bachelor's degree in electrical and computer engineering from King Abdulaziz University, Jeddah, Saudi Arabia in 2009, and the master's degree in Communication theory from the University of Tennessee, Knoxville, Tennessee, USA, in 2017.

Mr. Alharbi is currently a second year PhD student in the Department of Electrical and Computer Engineering at the Ohio State University working in the ElectroScience Laboratory, Columbus, OH, USA. He is sponsored by the King Abdulaziz City for Science and Technology (KACST) to pursue a Ph.D. degree in electrical and computer engineering. His current research interests include reconfigurable, flexible, and wearable antennas and wireless communications. He joined KACST, Riyadh, Saudi Arabia as a researcher engineer from 2009 to 2015. He worked with soft machines Inc., Santa Clara, USA from 2010 to 2013 on a joint project.



Qiji Ze received the B.S. and Ph.D. degrees in electrical engineering from Xi'an Jiaotong University, Xi'an, Shaanxi, China, in 2011 and 2018. He is currently working as a postdoctoral researcher at The Ohio State University and the Soft Intelligent Material Laboratory, Columbus, OH, USA. His research interests include magnetic-responsive soft materials and soft robotics.



Ruike Zhao received the B.S. degree from Xi'an Jiaotong University, Xi'an, China and the M.S. and Ph.D. degree from Brown University, Providence, RI, USA in 2014 and 2016, respectively, all in mechanical engineering. Before she joined The Ohio State University, Columbus, OH, USA as an Assistant Professor in the Department of Mechanical and Aerospace Engineering in 2018, she was a Postdoctoral Associate at Massachusetts Institute of Technology, Cambridge, MA, USA. Her current research interests include magnetic-responsive soft materials, mechanics of soft materials, additive manufacturing, soft robotics, active metamaterial, bioengineering, and biomedical devices.

Dr. Zhao was a recipient of the Haythornthwaite Foundation Research Initiation Award from the Applied Mechanics Division in The American Society of Mechanical Engineers (ASME). She is currently serving as a member of the Composite Materials Technical Committee in The International Mechanical Engineering Congress and Exposition (IMECE). She organized symposiums on "functional soft composite materials - Design, Mechanics, and Manufacturing" at The International Mechanical Engineering Congress and Exposition and The Society of Engineering Science.

**Asimina Kiourti** (S'10, M'14, SM'19)

received the Diploma degree in electrical and computer engineering from the University of Patras, Patras, Greece, in 2008, the M.Sc. degree in technologies for broadband communications from University College London, London, U.K., in 2009, and the Ph.D. degree in electrical and computer engineering from the National Technical University of Athens, Athens, Greece, in 2013.

Dr. Kiourti is currently an Assistant Professor of Electrical and Computer Engineering at The Ohio State University and the ElectroScience Laboratory, Columbus, OH, USA. She has (co-)authored over 40 journal papers, 80 conference papers, and 7 book chapters. Her research interests include wearable and implantable sensors, antennas and electromagnetics for body area applications, and flexible textile-based electronics.

Dr. Kiourti has received several awards and scholarships, including the URSI Young Scientist Award for 2018, the IEEE Engineering in Medicine and Biology Society (EMB-S) Young Investigator Award for 2014, the IEEE Microwave Theory and Techniques Society (MTT-S) Graduate Fellowship for Medical Applications for 2012, and the IEEE Antennas and Propagation Society (AP-S) Doctoral Research Award for 2011. She is currently serving as an Associate Editor for the IEEE Transactions on Antennas and Propagation and the IEEE Journal of Electromagnetics, RF and Microwaves in Medicine and Biology.